

The role of flaws on crack growth in rock-like material assessed by AE technique

Quansheng Liu · Jie Xu · Xuewei Liu ·
Jingdong Jiang · Bin Liu

Received: 15 September 2014 / Accepted: 27 April 2015 / Published online: 20 May 2015
© Springer Science+Business Media Dordrecht 2015

Abstract Experiments for the rectangular rock-like samples (made of high-strength gypsum and water-cement ratio is 1) with two parallel pre-existing flaws subjected to uniaxial compression were carried out to further investigate the influence of varying flaw geometries on mechanical properties and crack coalescence behaviors. According to the tests results, eight crack types were characterized on a basis of the mechanisms of crack nucleation, formation and propagation, and seven coalescence modes occurred through the ligament, including S-mode, M1-mode, M2-mode, M3-mode, T1-mode, T2-mode and T3-mode. The AE and photographic monitoring techniques were adopted to further clarify the procedure of the crack coalescence and failure during uniaxial compression tests and in consequence the whole process of crack emergence, growth, coalescence and failure was recorded in real time. The results of AE technique revealed that the characteristics of acoustic emission energy associate with crack coalescence modes, and AE location method can emphasize the moments of crack occurrences and follow the crack growth until final failure. This study put forward better understanding of the fracture and failure

mechanism of underground rock engineering, like rock burst.

Keywords Rock-like samples · AE and photographic monitoring · Crack coalescence and failure · Real time · AE location method · Fracture mechanism

1 Introduction

Many instable disasters of fractured rock mass result from crack nucleation, propagation and coalescence, which have caused a mass of death and great loss of material fortunes. Therefore, the research on fracture and failure mechanism of rock-like brittle materials containing pre-existing flaws has a great academic significance in rock mechanics. Up to now, a lot of experimental studies (Brace and Bombolakis 1963; Hoek and Bieniawski 1965; Peng and Johnson 1972; Dey and Wang 1981; Petit and Barquins 1988; Shen et al. 1995; Germanovich and Dyskin 2000; Celestino et al. 2001; Wong and Einstein 2006; Yang et al. 2009; Zhao et al. 2010; Yang and Jing 2011; Haeri et al. 2013) have been performed to further investigate the fracture and failure mechanism in different natural or rock-like materials. With the purpose of investigating the crack coalescence behaviors, Bobet and Einstein (1998) performed experimental study on rock-like samples with two pre-existing flaws, which showed that coalescence and failure occurred concurrently in uniaxial compression, but coalescence appears sooner

Q. Liu (✉) · J. Xu · J. Jiang
School of Civil Engineering, Wuhan University,
Wuhan 430072, Hubei, People's Republic of China
e-mail: 704793796@qq.com

Q. Liu · X. Liu · B. Liu
Institute of Rock and Soil Mechanics, Chinese Academy
of Sciences, Wuhan 430071, Hubei,
People's Republic of China

than failure in biaxial compression. [Haeri et al. \(2013\)](#) carried out the uniaxial compression experiments on sandstone samples containing a single flaw, and identified nine different crack types, which are applied to research crack coalescence and failure mode. In order to research the mechanism of multi-crack interaction under the influence of chemical environment, [Feng et al. \(2009\)](#) conducted uniaxial experimental studies on limestone samples, which indicated that mechanism of crack propagation was effected by many factors, such as ionization density and rock constituents. [Park and Bobet \(2010\)](#) have found that the cracking characteristics of open flaws are similar to that of closed flaw, and the crack coalescence types in samples with closed flaws are related to the geometry. To further understand the mechanical behavior of rock masses, [Zhou et al. \(2014\)](#) have carried out experiments on man-made flawed rock-like materials, which revealed five crack types including wing crack, quasi-coplanar secondary cracks, oblique secondary cracks, out-of-plane tensile cracks and out-of-plane shear cracks. Besides physical experimental studies, numerical simulation is also widely applied in the crack coalescence research, such as NMM, DDA, RFPFA, PFC and so on.

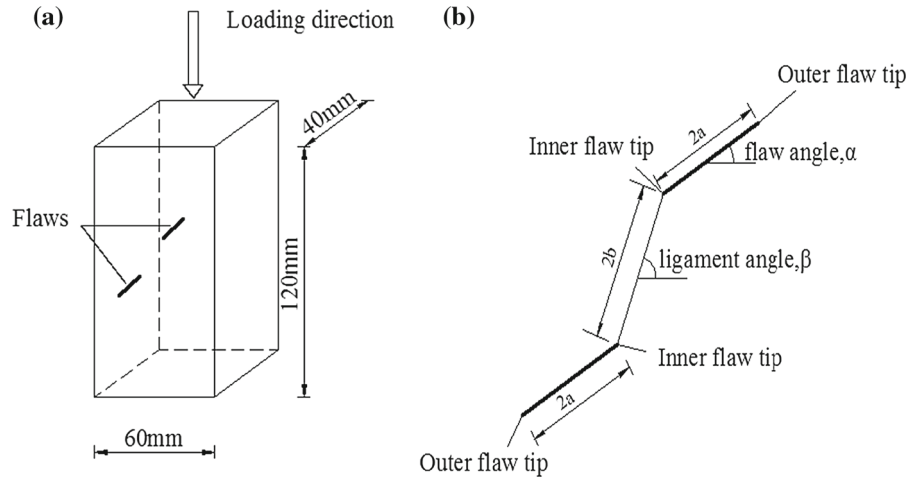
To describe accurately the cracking process in material is very challenging. Because several parameters including crack growth orientations, its growth rate and the coalescence mode under a given loading way should be fully measured and well assessed. It is well known that AE technique can monitor the transient response of each cracking occurrence and follow the crack growth until failure using transducers fixed on the surface of the material. The information obtained by AE can be used to reflect the cracks' location and the propagation behaviors. So far, AE technique has been widely applied to study the cracking behaviors and mechanism in many researches ([Lei et al. 1992](#); [Lockner 1993](#); [Pettitt 1998](#); [Cai et al. 2001](#); [Landis and Baillon 2002](#); [Colombo et al. 2003](#); [Schiavi et al. 2011](#); [Carpinteri et al. 2012](#)). [Li et al. \(2005\)](#) performed an experimental study on the acoustic emission behavior of pre-cracked marble samples, suggesting that AE counts increased rapidly near failure which accounted for nearly half of the total during the whole cracking process. [Tham et al. \(2005\)](#) summarized and presented the observations on the fracture shape and AE behavior of the tensile test samples, which revealed that the differences in frac-

ture shape and AE behavior were closely related to the heterogeneity of rock. [Jerome et al. \(2009\)](#) conducted experimental studies to investigate the acoustic emission signature of three axisymmetric compression experiments, and a significant similarity in AE behavior was found between compaction localization and cataclastic compaction, but shear localization was different. For the sake of studying the acoustic emission behaviors of cracking activity, [Sagarl et al. \(2013\)](#) performed three point bend tests on quasi-brittle materials using the AE system, which showed that AE behavior of each stage were greatly affected by the number and size distribution of pre-existing flaws. [Yang et al. \(2014\)](#) obtained the relationship between AE behavior and triaxial deformation of red sandstone during multi-stage triaxial compression, which showed AE events after peak strength were more active and mainly distributed in the local area of the potential damage plane.

However, very few experimental study have been performed about the characterization of the crack extension process and quantitative damage evaluation based on the analysis of received AE signals, especially regarding the rock-like materials containing pre-existing flaws. AE technique plays an important role in detecting the evolution and propagation of cracks in materials, but it is not enough. The acoustic waves are recorded mainly by the AE transducers from the inside. Photographic monitoring is a kind of optical and non-contact measurement technique, which has extensively been used to record the cracking process and determine the crack types. Up to now, AE and photographic monitoring techniques were less simultaneously applied to explore the cracking mechanisms of brittle rock containing pre-existing flaws.

This study provided an increasing understanding of coalescence behavior between two flaws in rock-like samples. For the sake of better understanding the strength failure and characterization of the crack process in rock materials, AE technique was adopted to the uniaxial compression tests. The crack coalescence process was recorded in real time in the whole deformation failure, which was not performed for rock-like materials previously. What's more, the cracking types, characteristics of crack coalescence, and strength of the samples were analyzed based on the combination of interior (AE technique) and exterior recording techniques (photographic monitoring).

Fig. 1 Sample with two flaws. **a** Overall view, **b** geometry of the flaws



2 Sample preparation and testing

2.1 Sample preparation

In order to carry out experimental study on mechanical properties and crack coalescence behavior of rock-like materials, the samples were made of high-strength gypsum and water–cement ratio is 1. The reason for choosing gypsum as modelling material is that a wide range of brittle rocks can be easily prepared and the experimental results can be conveniently compared with the previous studies. Besides, the overall dimensions of the samples were 60 mm wide \times 120 mm long \times 40 mm thick (see Fig. 1a). The height–width ratio of the samples is set to 2.0 to guarantee a uniform stress state in all samples interior (Fairhurst and Hudson 1999). The geometry of gypsum samples with two parallel flaws is depicted in Fig. 1b. The flaw geometry is described by four parameters: flaw length $2a$, ligament length $2b$, flaw angle α , and ligament angle β . With the purpose of illustrating the influence of pre-existing flaws on the cracking mechanisms, two flaw angles and six ligament angles were designed, while flaw length $2a$ and ligament length $2b$ were held constant, which were fixed at 14 and 16 mm, respectively. The chosen flaw angles were 45° and 75° , and the chosen ligament angles were 45° , 60° , 75° , 90° , 105° and 120° . The distances between two pre-existing flaws and the boundaries of samples were set in a reasonable range to eliminate the influence of side boundaries on the testing results. In order to ensure the accuracy of the test, three samples with same geometry were prepared. The final results were obtained based on the consis-

tency for two or three of samples with same geometry.

Each sample was cast in a mold, of which internal dimensions were set to 60 mm \times 40 mm \times 120 mm. Meanwhile, the open flaws were produced with different-sized metallic shims, which are 0.2 mm in thickness, 60 mm in length and 10–30 mm in width. The preparing process of samples with pre-existing flaws was as follows: (1) Put the moulds on the organic glass after assembly and coat soap-suds on the inwall in order to dismantle moulds easily. (2) Weigh water and gypsum powder accurately, stir well and then pour the mixture into the moulds quickly. Level the surface with a knife. (3) The thin metallic shims are set in specific locations to produce flaws before initial setting of gypsum. (4) Dismantle the moulds and cure samples under natural conditions for a month (see Fig. 2). Besides, the physic-mechanical parameters of intact samples are described in Table 1. σ_c is the uniaxial compressive strength, which is measured by cylindrical sample uniaxial compression tests; σ_t is the tensile strength, which is measured by Brazilian splitting tests; ϕ and c are measured by the triaxial compression test, which are respectively defined as frictional angle and cohesive force; K_{IC} is the fracture toughness, which is measured by the well-known Cracked Chevron Notched Brazilian Disc (CCNBD) test (Fowell et al. 1995).

2.2 Test equipment and procedure

The uniaxial compression experiments were performed using a RMT-150C servo-controlled testing machine

Fig. 2 Preparing process of samples with pre-existing flaws. **a** Casting samples. **b** Making flaws. **c** Curing samples. **d** Standard samples

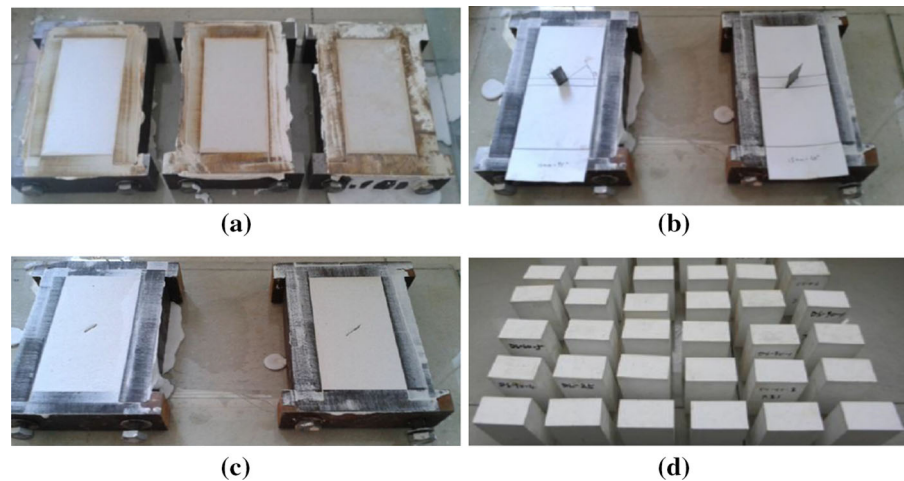


Table 1 Physico-mechanical parameters of intact samples

σ_c (MPa)	σ_r (MPa)	E (GPa)	c (MPa)	φ (°)	ρ (g/cm ³)	K_{IC} (MPa · m ^{1/2})
5.45	0.90	1.30	2.44	9.03	0.84	0.65

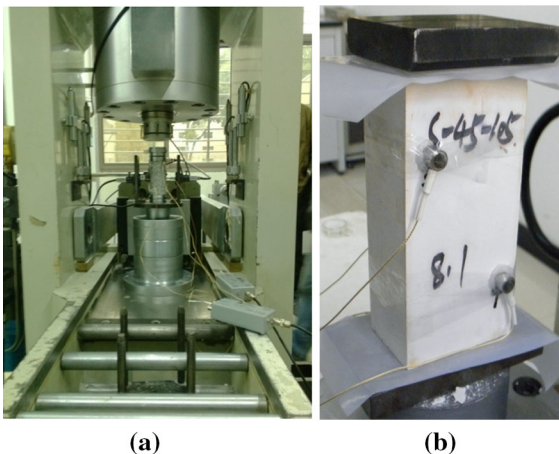


Fig. 3 RMT-150C rock mechanics servo-controlled testing system. **a** RMT-150C. **b** Experimental setup for the sample

in the Institute of Rock and Soil Mechanics, Chinese Academy of Sciences, as shown in Fig. 3. This testing system can record stress and strain data automatically and analyze the relationship of them in real time. All samples were loaded under uniaxial compression with a strain rate of 1×10^{-3} mm/s. Moreover, in order to obtain the real-time cracking process of the rock-like samples, the PCI-2 AE testing system (produced by American Physical Acoustic Corporation) was adopted to our experiments, as shown in Fig. 4. It is generally known that AE testing has been widely employed in

dynamic inspect and research of fracture behavior of materials in real time. In our tests, the amplitude threshold was set at 40 dB to improve signal to noise ratio. The sampling frequency and the sampling length were fixed at 2.5 MHz and 8192, respectively. The type of the sensors was Nano30, of which the operating frequency is 100–400 kHz. The sensors were coated with Vaseline—a coupling agent, and fixed on the surface of the samples by plastic tapes. To ensure the coupling effect of the AE sensor with the sample, a pencil lead break (PLB) should be performed before the tests began. In addition, a high-speed video camera called HG-100K was used in our experiments, which has the collection, testing, analysis and other integrated functions. HG-100K was equipped with a 1.7 million pixel COMS image sensor, of which the maximum resolution was 1504×1128 pixels. Moreover, the frame rate can range from 25 to 1,00,000 fps according to specific conditions. The time spacing during loading process was closely related to the actual resolution and frame rate.

3 Mechanical properties of flawed samples

The axial stress–strain curves of rock-like samples containing varying flaw geometries subject to uniaxial compression stress were illustrated in Fig. 5. We

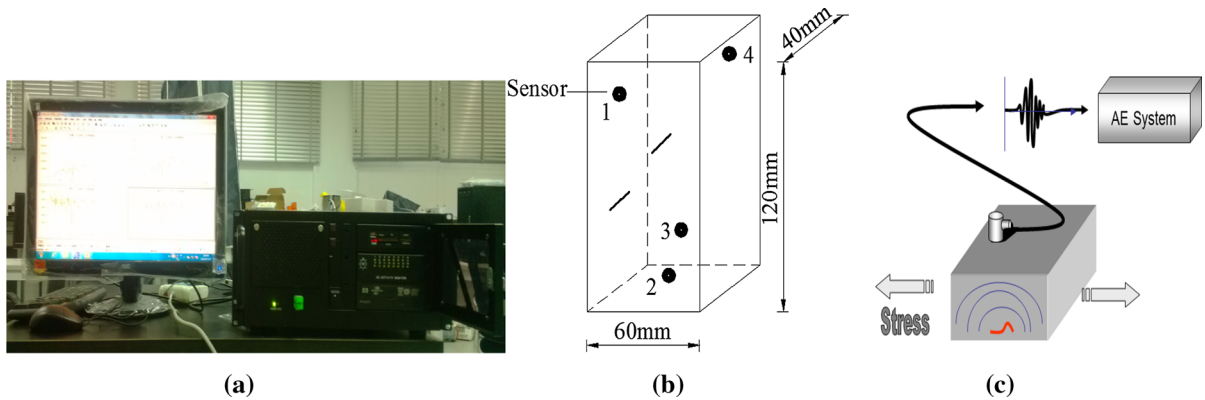


Fig. 4 AE PCI-2 acoustic emission system. **a** AE PCI-2. **b** Setup for sensors. **c** Operation theory of AE system

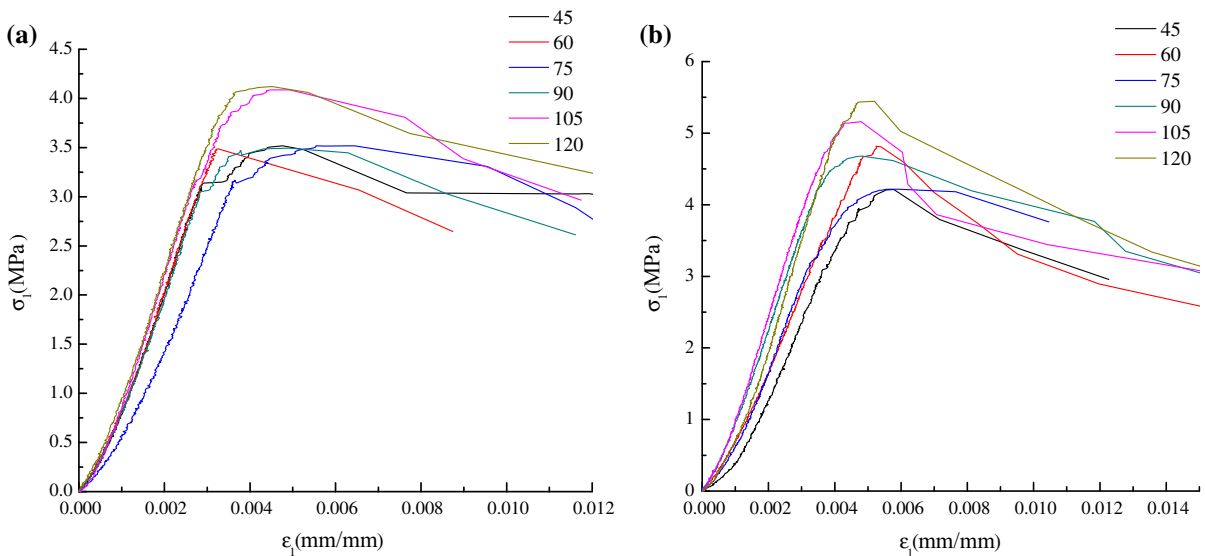


Fig. 5 Axial stress–strain curves of flawed samples, in which **a** and **b**, separately, illustrate the flaw angle **a** $\alpha = 45^\circ$ and **b** $\alpha = 75^\circ$

can come to the conclusion that two key parameters of the flaw (flaw angle α and ligament angle β) greatly affect the mechanical properties of the flawed samples. We will elaborate this problem in greater detail in the following.

3.1 Axial stress–strain curves of the samples containing varying flaw geometries

The whole stress–strain curve consists of four distinct phases: flaw closure phase, elastic deformation phase, nonlinear hardening phase, and strain-softening phase. At the initial stage of axial compression, the

relationships between stress and strain of flawed samples all show the downward concave, which also can be referred to as initial compaction phase. The reason for these is that it is owing to the closure of primary defects. Moreover the rigidity of all samples at flaw closure stage has better consistency, which roots in better homogeneity of experimental materials. And when the stress increases, the experimental material exhibits a largely linear stress–strain behavior in spite of some irrecoverable deformation including flaw closure and crack initiation. This process is known as elastic deformation. What’s more, the slope of the line in the stress–strain curve is bound up with ligament angle β . For instance, it can be seen in Fig. 5b that the

slope of the line increases with the increase of ligament angle β . When entering the nonlinear hardening phase, the relationship between the stress and strain obviously shows the non-linear character. This means that new cracks begin to initiate and propagate, that is always resulted by the stress concentration at the flaw tips. In accordance with Fig. 5, the peak strengths of samples containing greater ligament angle such as $\beta = 105^\circ$ or 120° are obviously higher than those of others, so one main result emerges that it is harder to fail for overlapping flaw geometries ($\beta \geq 90^\circ$) compared with the non-overlapping ($\beta \leq 90^\circ$). When the stress–strain curves reach the fourth stage—that is what we call the “strain-softening”, the macroscopic cracks appear in the samples which lead to the performance degradation and failure of the sample. Meanwhile, the post-peak stress–axial strain curves show a gentle fall.

3.2 Influence of flaw geometries on the sample mechanical properties

The effect of flaw geometries on the sample mechanical properties such as strength and deformation characters will be elaborated in this section. The research results may provide theoretical foundation for the investigation of the cracking mechanism of fractured rock mass in underground engineering.

In accordance with Table 1, the uniaxial compressive strength of intact sample is 5.450 MPa. A comparison between intact samples and flawed samples of uniaxial compressive strength indicates that the average reduction extent for the samples with $\alpha = 45^\circ$ or $\alpha = 75^\circ$ is 32.02 or 12.76%, respectively. Furthermore, the uniaxial compressive strength of the samples containing flaw angle $\alpha = 75^\circ$ is significantly higher compared with those with flaw angle $\alpha = 45^\circ$, demonstrating neatly how the samples with flaw angle $\alpha = 75^\circ$ can build higher levels of compression strength. Moreover, when the β angle is increased from 45° to 75° and from 45° to 90° for α angle 75° and 45° respectively, the uniaxial compressive strength remains flat. Then it trends to increase with increasing of ligament angle and the demarcation point is $\beta = 90^\circ$ for $\alpha = 45^\circ$, and $\beta = 75^\circ$ for $\alpha = 75^\circ$.

But when it comes to the apparent elastic modulus of flawed samples, a different change rule is shown in Fig. 6b compared with the uniaxial compressive

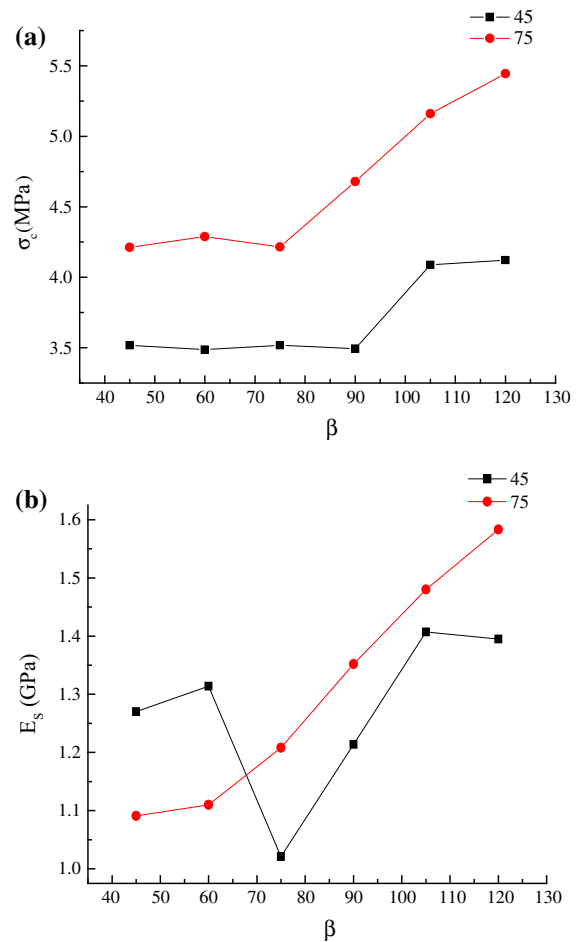


Fig. 6 Effect of flaw angle and ligament angle on mechanical properties of samples. **a** Uniaxial compressive strength. **b** Elastic modulus

strength. For the samples with $\alpha = 45^\circ$, there is a distinct valley at the point of $\beta = 75^\circ$, then the apparent elastic modulus curve keeps a sustaining growth with the increasing ligament angle and the demarcation point is $\beta = 90^\circ$. However, unlike samples with $\alpha = 45^\circ$, the apparent elastic modulus curve of samples with $\alpha = 75^\circ$ shows a growing tendency from beginning to end, which has almost no sudden turning point.

The above experimental results reveal that the flaw geometric parameters of the samples including flaw angle α and ligament angle β greatly affect the strength and deformation behaviors. In addition, when $\beta \geq 90^\circ$, all mechanical parameters increase with increasing ligament angle, which shows that the overlapping flaw geometries have contributed more to the stability of the samples.



Fig. 7 Axial splitting failure of intact rock-like sample

4 Crack coalescence behavior

In addition to mechanical properties, cracking behavior for flawed materials and structures is a valuable

research issue, which involves crack initiation types and crack coalescence modes. As indicated in Fig. 7, the intact sample took on axial splitting tensile failure and the crack propagation direction was consistent with the loading direction. That is a typical failure mode for brittle materials subject to uniaxial compression. In comparison, different crack initiation types and coalescences modes were observed from the flawed samples, which were sensitive to both the ligament angle and flaw angle. This section focuses on a further investigation on cracking behaviors in flawed samples.

4.1 Crack types of flawed sample

Figure 8 presents eight different crack types observed during the sample cracking progress, which were defined based upon their initiation mechanism and trajectories subject to the applied loading. In accordance with Fig. 8, one can see that T type is divided into four types (T type-I, T type -II, T type -III and T type -IV) according to its geometry and initiation mode, whose

Fig. 8 Eight crack types observed in the experiments

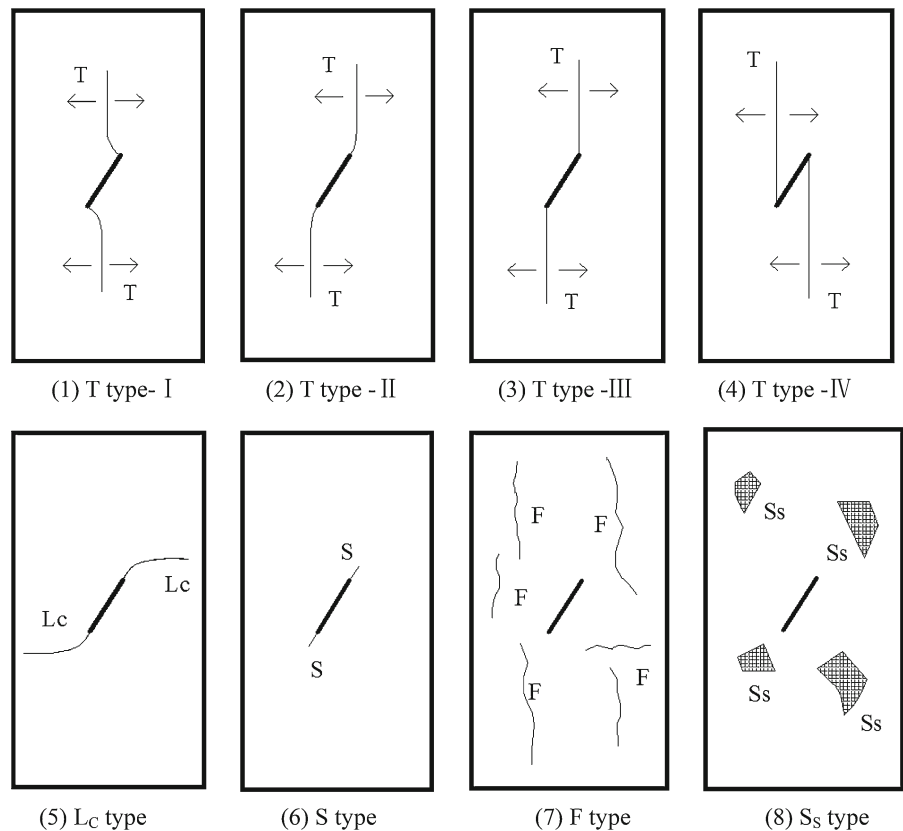


Fig. 9 Failure modes of the samples containing different flaw geometries.

a $\alpha = 45^\circ, \beta = 45^\circ$.

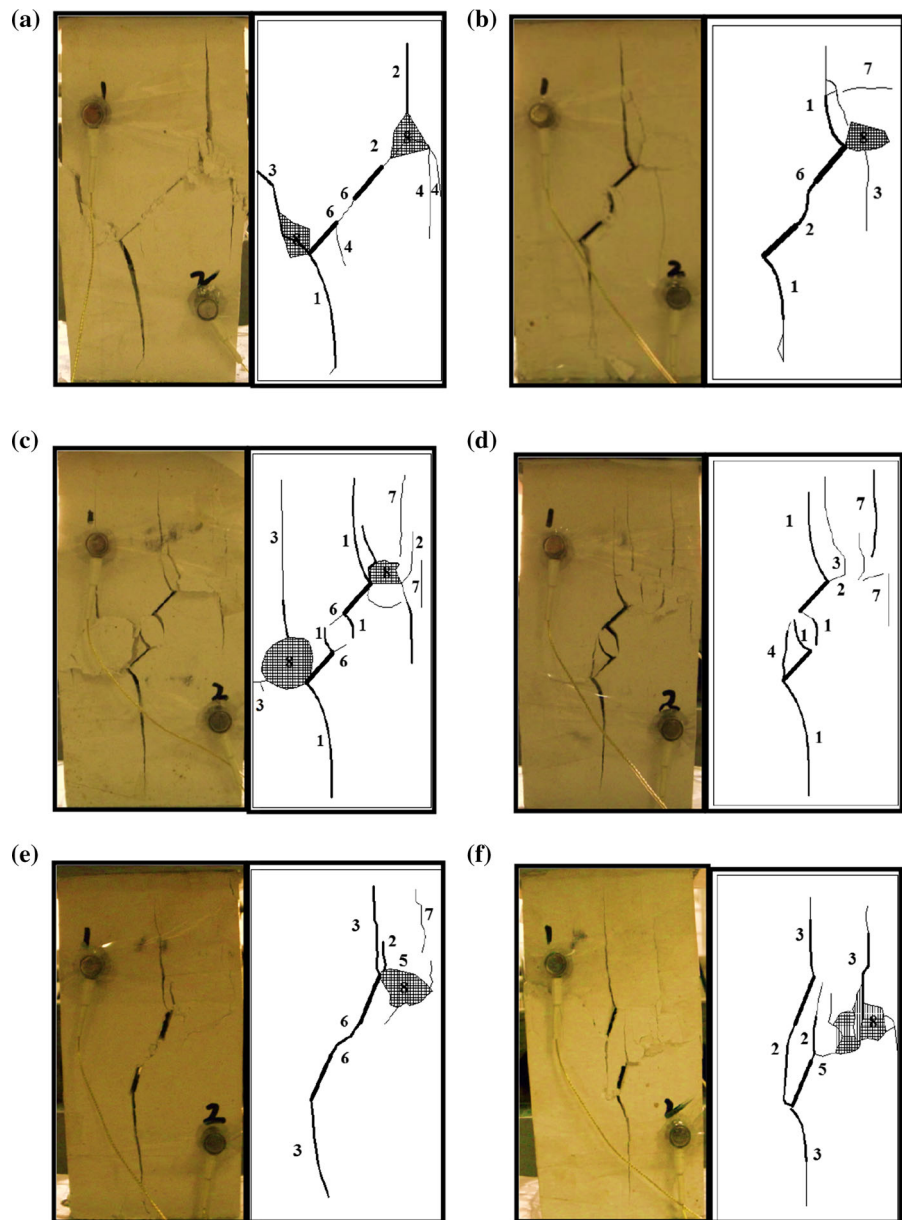
b $\alpha = 45^\circ, \beta = 60^\circ$.

c $\alpha = 45^\circ, \beta = 75^\circ$.

d $\alpha = 45^\circ, \beta = 105^\circ$.

e $\alpha = 75^\circ, \beta = 60^\circ$.

f $\alpha = 75^\circ, \beta = 120^\circ$.



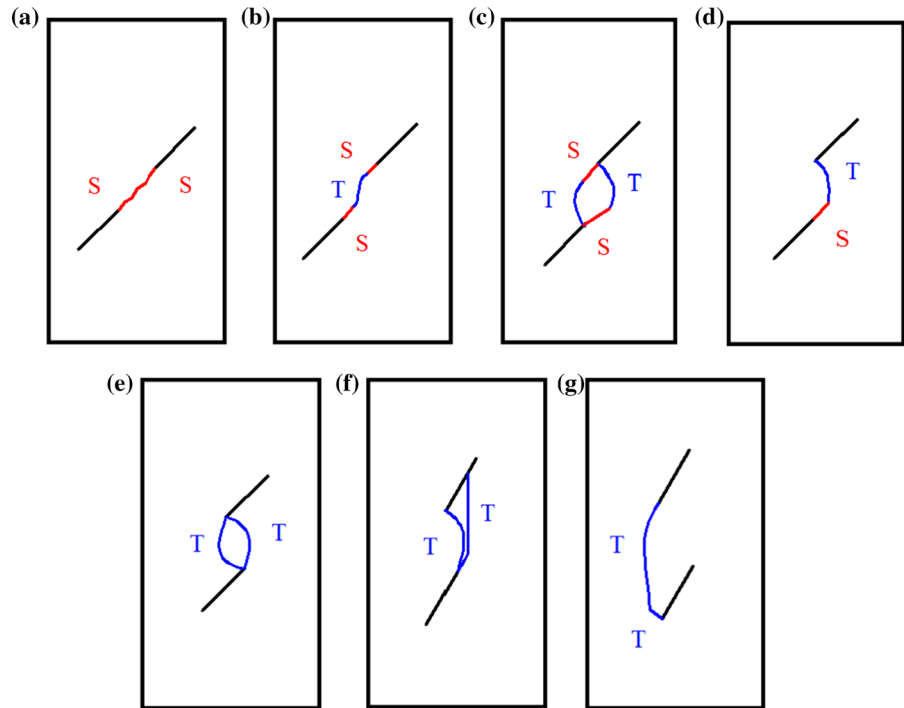
general character is tensile crack. Besides, L_C type is lateral crack, S type is shear crack, F type is far-field and S_S type is surface spalling.

The above eight crack types can be used to investigate the crack coalescence mode and failure mechanism during the sample cracking progress, which may contribute to study rock damage and fracture mechanism. The ultimate failure modes containing above various crack types for flawed samples were shown in Fig. 9.

As indicated in Fig. 9, various cracks among the above eight crack types cover every sample's surface, of which size and location vary wildly. Take the sample ($\alpha = 45^\circ, \beta = 45^\circ$) for example, its ultimate failure mode is a combination of cracks T type I–IV, S type and S_S type. The characters of the crack initiation and propagation of above eight crack types were summarized through observation as follows. T type-I, T type-II and T type-III are typical tensile cracks, which are easily recognized because of the clean and smooth surface.

Fig. 10 Seven patterns of crack coalescence.

a S-mode. **b** M1-mode.
c M2-mode. **d** M3-mode.
e T1-mode. **f** T2-mode.
g T3-mode



T type-I is initiated as the first crack from the flaw tips only when the flaw angle is equal to 45° , while T type-III is usually found as the main crack in the sample for $\alpha = 75^\circ$, such as $\alpha = 75^\circ$ and $\beta = 60^\circ$. Moreover, T type-I is observed to originate from the inner tips of the flaws when β ranges from 75° to 105° , whereas for $\beta = 120^\circ$, T type-II usually is initiated at the inner tips of the flaw. It reveals that the crack type is sensitive to both the flaw angle and ligament angle. T type-IV, in contrast, is reverse to the T type-III in response to the applied loading and referred to as “anti-tensile crack”, which is usually initiated as later crack following with T type-I and T type-III. L_C type (Lateral crack) is most commonly found in the samples containing $\alpha = 75^\circ$ such as Fig. 9e and f, which means flaw angle $\alpha = 75^\circ$ makes the sample easier to develop L_C type in the two-flaw geometries. L_C type initiates firstly from the flaw tips, and then propagates progressively with a smaller inclination angle towards the horizontal direction until expanding to the side boundary of sample. It is worth mentioning that the trajectory of S type (shear crack) initiation and propagation is parallel to the pre-existing flaw, which mainly occurs when the ligament angle β is less than or equal to 75° . Unlike these tensile cracks, the propagation of S type is driven by shear stress. The initiation point of F type (far-field crack) is uncertain,

as well as the propagation trajectory, which may be linear or curvilinear. Besides, S_S type (surface spalling) generally occurs as the latter crack to accompany with several tensile cracks, and can be found in almost all the samples.

4.2 Crack coalescence and AE behaviors of the samples containing different geometries

Section 4.1 mainly summarized two typical cracks, i.e. T type crack and S type crack. T type crack is tensile in nature that initiates on an angle to the flaw and propagates along the loading direction, whereas S type crack usually initiates parallel to the pre-existing in response to shear stress. According to the experimental results, seven modes of crack coalescence obtained in the cracking process were defined based on the combination of above two crack types, which can be classified as (1) shear crack coalescence [S-mode in Fig. 10a], (2) mixed shear/tensile crack coalescence [M-mode in Fig. 10b–d] or (3) tensile crack coalescence [T-mode in Fig. 10e–g]. It is noteworthy that each crack coalescence has a specific AE behavior pattern. As indicated in Table 2, the various crack coalescence modes for all testing flawed samples were shown.

Table 2 Crack coalescence modes of flawed samples with different geometries

Sample	$\alpha/^\circ$	$\beta/^\circ$	S-mode	M1-mode	M2-mode	M3-mode	T1-mode	T2-mode	T3-mode
1	45	45	**						
2	45	60	*	*					
3	45	75		*	*				
4	45	90				*	*		
5	45	105					*	*	
6	45	120						*	*
7	75	45	**						
8	75	60	**						
9	75	75	**						
10	75	90				*	*		
11	75	105					*	*	
12	75	120						*	*

* Crack coalescence occurs in the corresponding mode

4.2.1 S-mode crack coalescence

For S-mode crack coalescence, tensile crack usually appears as the first crack at the flaw tips. Before the further growth of tensile cracks, shear cracks begin to originate from the inner tips and then grow in a direction parallel substantially to the flaw, but they soon expand along own path forward until coalescence. Consequently, S-mode crack coalescence occurs in the ligament by the connection of two shear cracks, while the outer tensile cracks go on propagating until the edges. As indicated in Table 2, one can conclude that S-mode coalescence is produced when the two flaws are almost colinear, which is in the condition of $\beta \leq \alpha \leq 75^\circ$.

According to Fig. 11, a further study to look into the AE activity law of S-mode coalescence was conducted. The AE behavior pattern of S-mode coalescence consists of three stages: minor active stage, quiet stage and major active stage. At the beginning of the axial compression, the AE events emerge and show a little active, which is owing to the closure of primary defects. The initial AE activity process subject to the applied loading is defined as the minor active stage, which corresponds to flaw closure phase of the stress–strain curve. With the increase of applied load, AE behavior enters into the second stage, i.e. the quiet stage. During this process, the AE behavior is more stable compared with the active period and accompanied with the elastic deformation of the flawed samples. When the AE energy increase continuously and show denser than before,

they start to enter the major active stage. The reason for this is that, new cracks initiate from the flaw tips and the samples produce nonlinear elastic deformation.

The blue dots marked in Fig. 11 correspond to the point of the first crack initiation in the flawed samples. For the sample with $\alpha = 45^\circ$ and $\beta = 45^\circ$, the time of the first crack initiation is at 270s and the axial stress is 2.25 MPa, which is approximately similar to that of the sample with $\alpha = 75^\circ$ and $\beta = 75^\circ$ ($T = 270\text{s}$, $\sigma_{t1} = 2.26\text{ MPa}$) (σ_{t1} represents the crack initiation strength). However for the sample containing $\alpha = 75^\circ$ and $\beta = 45^\circ$ as shown in Fig. 11b, the AE behavior is different whereby the time of crack initiation is at 380s and the axial stress is 3.15 MPa, which results from $\alpha \neq \beta$. When the flaw angle α is not equal to the ligament angle β , the crack growth will be hindered by the changes in the direction of the shear crack propagation. Consequently, a lot of crushed gypsum powder can be observed from the failure picture of the sample with $\alpha = 75^\circ$ and $\beta = 45^\circ$. Notice, in Fig. 11a, the AE energy firstly begins to decrease at 380s, and then increases with the increase of applied load, which results from the sudden appearance of cracks extending to the vertical edges (Fig. 9a).

4.2.2 M-mode crack coalescence

The M crack coalescence is classified as three types, i.e. M1-mode coalescence, M2-mode coalescence and M3-mode coalescence. For the M1-mode coalescence

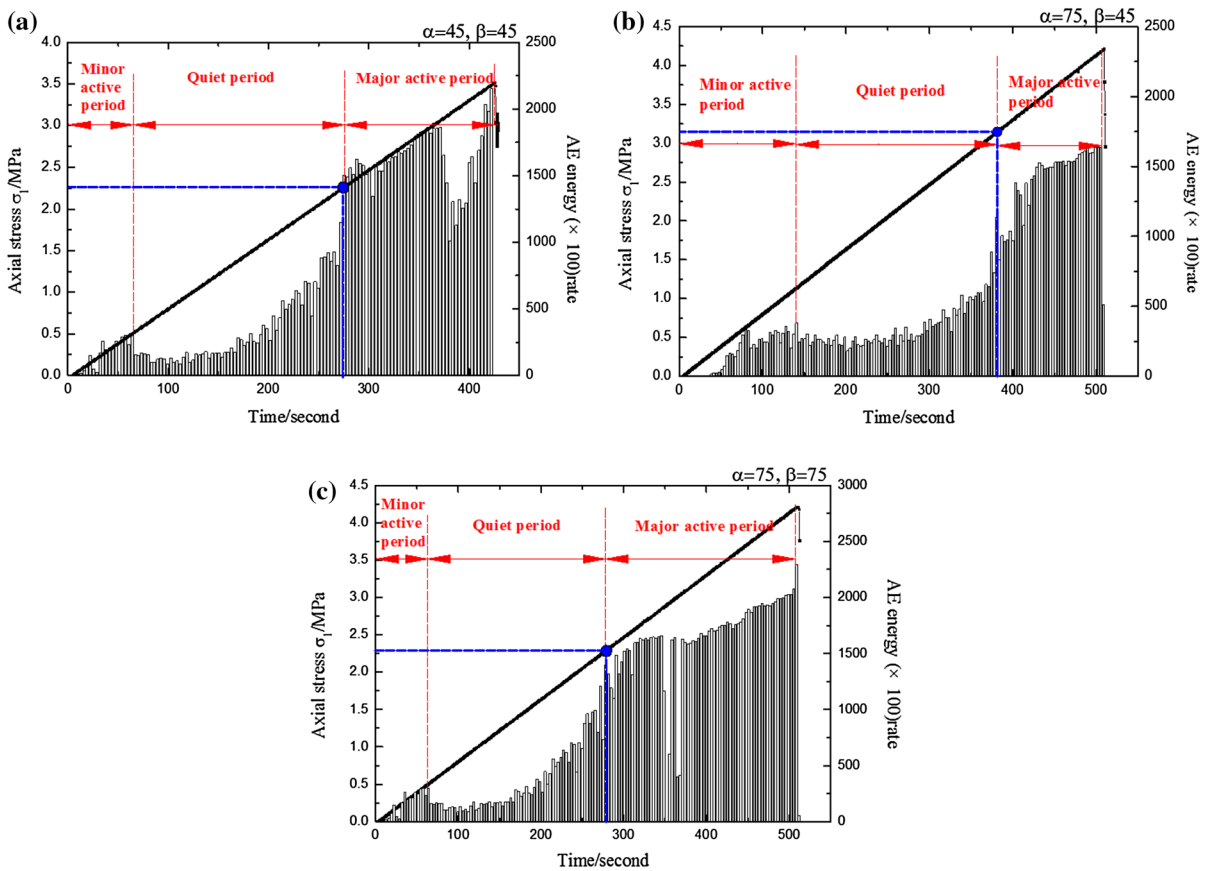


Fig. 11 AE energy and axial stress of flawed samples in S-Mode coalescence

(see Fig. 10b), a tensile crack is the first to occur in the ligament. Before the tensile crack further expanding, two shear cracks originate simultaneously from inner tips of two pre-existing flaws. As the shear cracks propagate further, M1-mode coalescence appears suddenly in the ligament with the shear cracks linking the upper and lower tips of tensile crack. For the M2-mode coalescence shown in Fig. 10c, two tensile cracks originate simultaneously from inner tips of two flaws, and then grow through most parts of the ligament. During the process of tensile crack propagation, two shear cracks also initiate from inner tips, and propagate along the flaw direction. The M2-mode coalescence will be abruptly generated by two shear cracks linking the coming tensile cracks. For the M3-mode coalescence (see Fig. 10d), the upper tensile crack first initiates and propagates on an angle to the flaw, then the M3-mode coalescence occurs by a shear crack connecting the lower pre-existing crack and the tip of the tensile crack.

According to the statistic results in Table 2, one can conclude that the M-mode coalescence occurs when $60^\circ \leq \beta \leq 90^\circ$ and the tensile crack may become dominant with the increase of the ligament angle. Moreover, our observations suggest that the surface of the sample producing M-mode coalescence consists of two evident areas: a rough area covered with crushed gypsum powder that demonstrates shearing, and a smoother area that demonstrates its nature in tension (Bobet and Einstein 1998).

4.2.3 T-mode crack coalescence

The T-mode crack coalescence is classified as three main modes T1, T2 and T3. As indicated in Fig. 10e, the T1-mode coalescence occurs when two tensile cracks nucleate from inner tips of the flaws, propagate through the ligament, and then link with the inner tip of the other flaw. The isolated area formed by two tensile

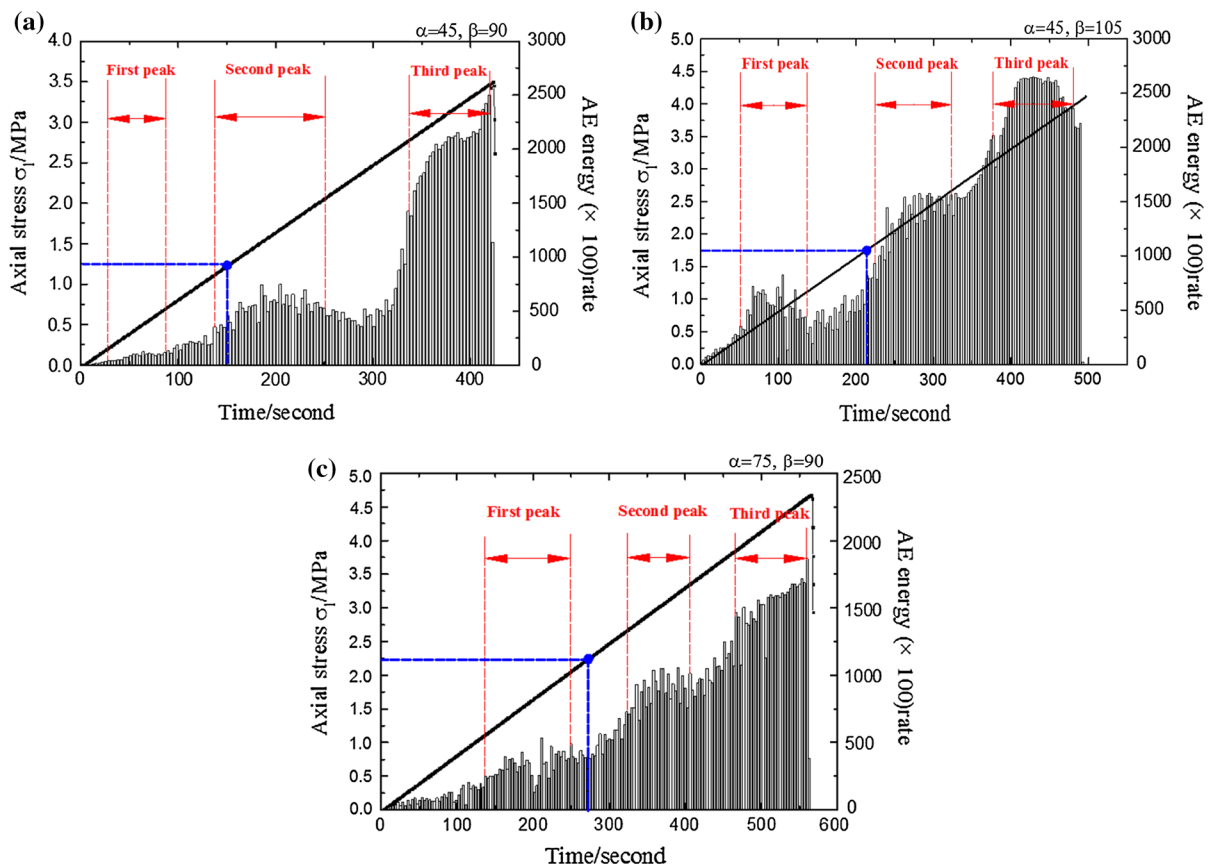


Fig. 12 AE energy and axial stress of flawed samples in T1-Mode coalescence

cracks in the ligament is usually described as “fish eye”. For the T2-mode coalescence shown in Fig. 10f, two tensile cracks also initiate simultaneously from inner tips of two flaws, but the lower one grows further by its own path until it reaches some point of the upper flaw except for the tips and, at the same time, the other expanding tensile crack links with the inner tip of the lower flaw. For T3-mode coalescence shown in Fig. 10g, a tensile crack generally emanates from the inner tip of the upper flaw, and then T3-mode coalescence emerges with a sudden occurrence of the propagating tensile crack linking with the outer tip of the lower flaw. One can conclude from Table 2 that the T-mode coalescence usually occurs when $\beta \geq 90^\circ$, which is the geometry of the overlapping. The T-mode coalescence is the simple combination of two tensile cracks and, in consequence, the surface of the sample producing T-mode coalescence is cleaner and smoother compared with S-mode and M-mode.

According to Fig. 12, a detailed investigation of the internal connection among AE activity law and the T1-mode coalescing process is performed. Based on the AE energy shown in Fig. 12a–c, the AE behavior pattern of the sample producing T1-mode coalescence is characteristic by three various peaks, a distinct difference comparing with the S-mode coalescence (Fig. 11). The first peak period corresponds to the minor active period of the S-mode coalescence, which is also caused by the closure of pre-existing flaws and natural fractures. However, it’s worth mentioning that new tensile cracks in the ligament begin to originate from the flaw tips during second peak period. Due to the rapid and severe propagation of the tensile cracks, the AE behavior becomes so active that the second peak forms. With the increase of the applied load, the cracks emanating from the outer tips of flaws continue propagating, until the sample fails with an appearance of a through crack. At the same time, more and more AE

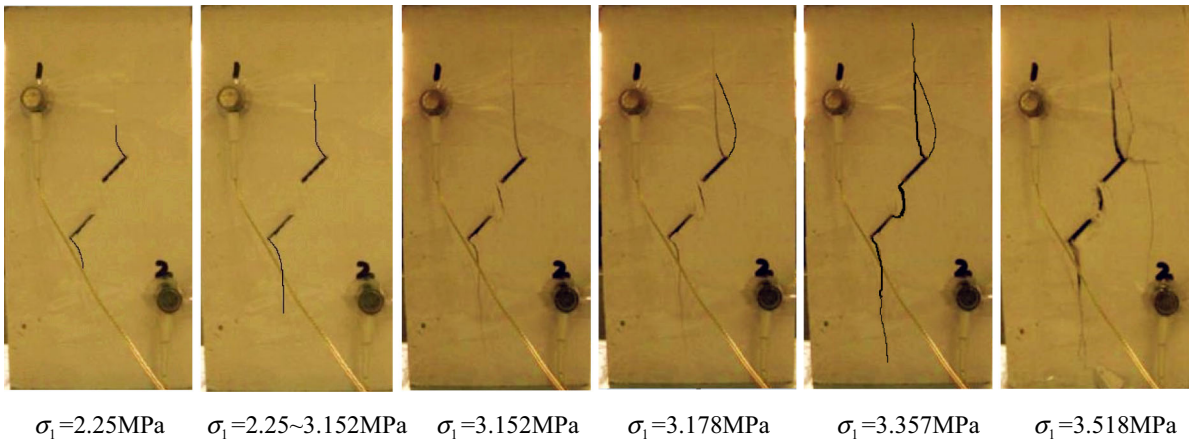


Fig. 13 Crack coalescing process of flawed sample ($\alpha = 45^\circ, \beta = 75^\circ$)

events are produced during the cracking process, and that is the third peak period.

In accordance with the blue marks in Fig. 12, one can conclude that the crack initiation stress of the sample with the T1-Mode coalescence is smaller compared with the S-Mode coalescence, which means that the flaw geometry producing T1-Mode coalescence makes it easier for the sample to develop the first crack. The underlying cause may be that it is easier for tensile cracks to initiate than shear cracks. For the flawed sample with $\alpha = 45^\circ$ and $\beta = 105^\circ$, the AE behavior is more active and the AE events are denser by comparing with the others. The reason, our research suggests, may be that the greater resistance from the overlapping flaw geometries ($\beta \geq 90^\circ$) make the cracks more difficult to propagate in the flawed samples.

4.3 Crack coalescing process obtained in real time

With the purpose of further investigating the crack coalescing process subject to the axial stress, an integrated methodology, which represents a combination of the AE location technique and photographic monitoring, was adopted in the experiments. By this method, the detailed process of the flawed sample producing crack coalescence is shown in real time and, in addition, several important phenomena and the corresponding reasons are described and analyzed, respectively.

Take the sample containing $\alpha = 45^\circ$ and $\beta = 75^\circ$ for example, a detailed description of its real-time crack

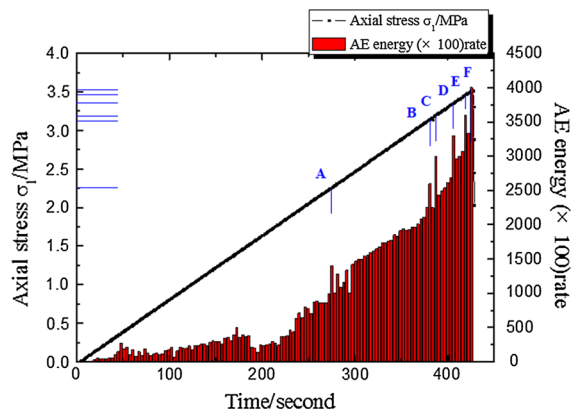
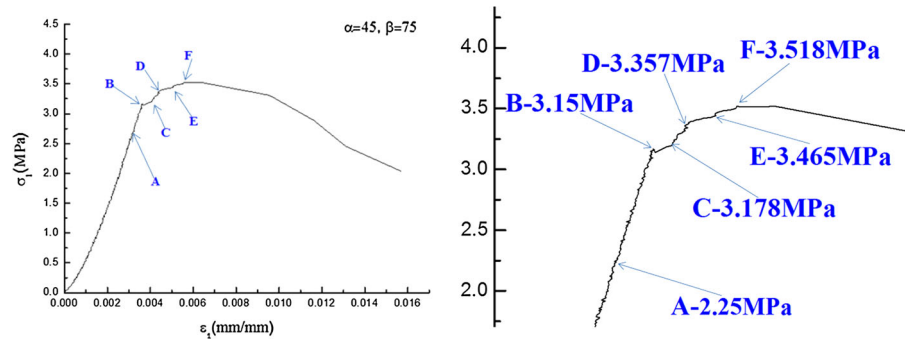


Fig. 14 The features of the AE energy during the cracking process ($\alpha = 45^\circ, \beta = 75^\circ$)

coalescence process is provided, which is indicated in Figs. 13, 14, 15. During the initial load, the deformations of the flawed sample undergo two stages: crack closure stage and elastic deformation stage, where the stress-strain curve shows the downward concave and the linear relationship, respectively. Based on the computation results shown in Fig. 16a, the average modulus is 1.09 GPa. Then two tensile cracks belonging to T type-I begin to initiate separately from the outer tips of flaws, which is induced by a high tensile stress concentration at the tips. The initiation moment corresponds to the point A ($\sigma_1 = 2.25 \text{ MPa} = 64\% \sigma_c$), where the axial stress is equal to 2.25 MPa, about 64 percent of the uniaxial compressive strength. Notice that the initiation of first crack is recorded by AE energy as well, as indicated in Fig. 14. With the increase of the applied

Fig. 15 Several important points in axial stress–strain curve ($\alpha = 45^\circ$, $\beta = 75^\circ$)



load, two T type-I tensile cracks go on propagating along the direction parallel to the applied load. However, owing to the irreversible damage of load-bearing structures, the average modulus is reduced from 1.09 to 1.0 GPa (Fig. 16b). When applied load increases to the first yielding point B ($\sigma_1 = 3.152 \text{ MPa} = 89.6 \% \sigma_c$), a vertical tensile crack appears suddenly in the ligament where a high tensile stress gathers and, in consequence, the axial stress produced a small but significant drop to 3.074 MPa from 3.152 MPa, which is clearly illustrated in Fig. 15. At the same time, our observations suggest that the boundary limitation of the testing sample results in the propagation of T type-I tensile cracks being hindered, which only widen a lot. Afterwards, the axial stress has a trend of slow increase, which reveals the supporting capacity of the sample is being strengthened gradually. When loaded to point C ($\sigma_1 = 3.178 \text{ MPa} = 90.3 \% \sigma_c$), the sample begins to initiate the T type-II crack from the outer tip of the upper flaw. Analysis found that the average modulus undergoes a distinct drop to 0.397 GPa from 1.0 GPa (Fig. 16c), which results from great damage of bearing structure. At the moment of the sample loaded to the second yielding point D ($\sigma_1 = 3.357 \text{ MPa} = 95.4 \% \sigma_c$), two shear cracks emanate concurrently from inner tips of two flaws and propagate along the direction parallel to the flaws, then it is followed by the sudden occurrence of the M1-Mode coalescence, which mainly results from the above two shear cracks joining the vertical tensile crack in the ligament. According to the AE results indicated in Fig. 14, it is quite clear that the above process is recorded by the AE technique as well. During this process, the axial stress–strain curve shows a more slowly increasing trend compared with the previous stage and, in consequence, the average modulus goes down to 0.117 GPa from the

previous 0.397 GPa (Fig. 16d), which is also caused by the irreversible damage deformation of the sample. When the applied load reaches 3.465 MPa ($98.5 \% \sigma_c$), several far-field cracks begin to initiate and propagate along the uncertain paths, and in the meanwhile, surface spalling are also observed on the surface of the sample. When the continuous increasing load gets to 3.518 MPa ($100 \% \sigma_c$), the T type-I tensile cracks that appear firstly propagate rapidly until reaching the upper and lower edge of the sample, which results in fragile failure mode. Then, it is followed with a sharp decline of the axial supporting capacity to 2.035 MPa.

According to Fig. 17, one can conclude that the AE location technique is an effective tool to embody the cracking process of flawed sample subject to the applied load. During the initiation of loading, the AE behavior is not active and AE events are relatively few in number, which means there is no rule to follow in the AE signature. When the applied stress increases to 2.25 MPa (point A), our analysis suggests that more AE events distributed at the outer tips indicate the appearance of T type-I tensile cracks. Statistics show that the AE events only accounts for 6.9% of the total. With the increase of the applied load, a red area emerges gradually in the ligament, and it shows where the vertical tensile crack appears. Afterwards, it is obvious that the increasing stress leads the AE events to increase rapidly. At the moment of about 406 s (corresponding axial stress is 3.357 MPa), the ligament is densely packed with AE events—more than in most regions of the sample (Fig. 17e), which indicates M1-Mode coalescence occurs. Statistics show that the current proportion of AE events has risen to 79.3%. When the sample is loaded to 3.518 MPa (corresponding time is 425 s), a red AE event form-

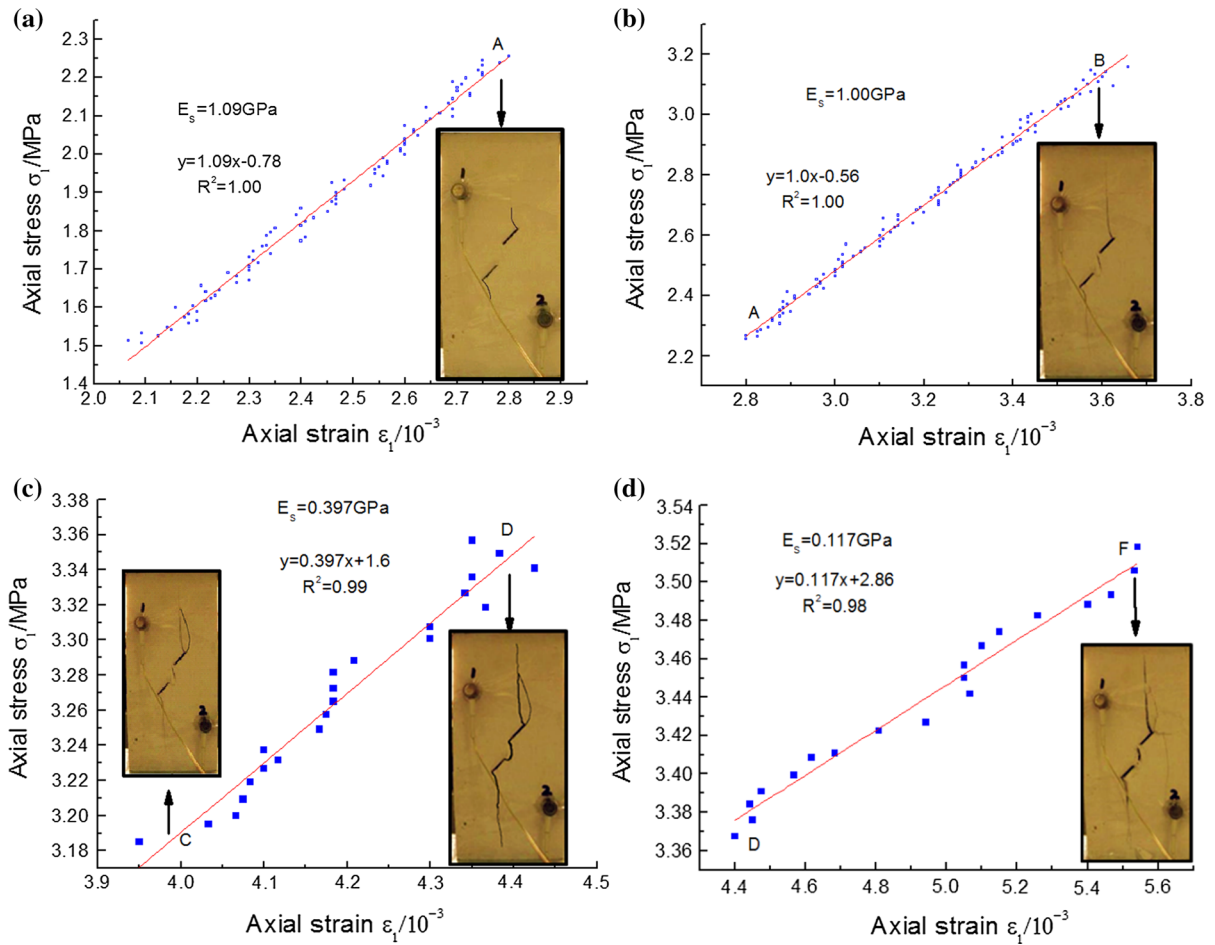


Fig. 16 Relationship between axial stress and strain

ing region that exists throughout the sample reveals that the testing sample fails, which is highlighted in Fig. 17g.

In our experiments, the crack coalescence and failure process of all samples were recorded in real time and analyzed in detail based on the combined application of photographic monitoring and AE technique, and in consequence two main results emerge: firstly, it is found that the axial stress-axial strain gradually deviates from the original track and develops towards the axial strain, which is caused by continuously increasing damage subject to the increasing load; secondly, it can be concluded that the bigger decline of the average modulus reveals the appearance of new cracks, which is accompanied with more active AE behavior, such as the larger AE energy and more AE events.

5 Conclusions

The experimental study aims at investigating the deformation and strength characters, crack coalescence mode and failure mechanism of the rock-like samples containing different flaw geometries subject to the axial applied load. An integrated methodology, which represents a combination of the AE location technique and photographic monitoring, was adopted in the experiments. The main research results are shown below.

1. A comparison between intact samples and flawed samples of mechanical parameters indicates both uniaxial compressive strength and apparent elastic modulus of flawed samples are lower than that of intact samples. Our observations suggest that

Fig. 17 Distribution of the AE events in cracking process

($\alpha = 45^\circ$, $\beta = 75^\circ$).

a
 $\sigma_1 = 1.69 \text{ MPa}$ ($T = 207 \text{ s}$;
 Before A).

b
 $\sigma_1 = 2.25 \text{ MPa}$ ($T = 274 \text{ s}$;
 Point A). **c**

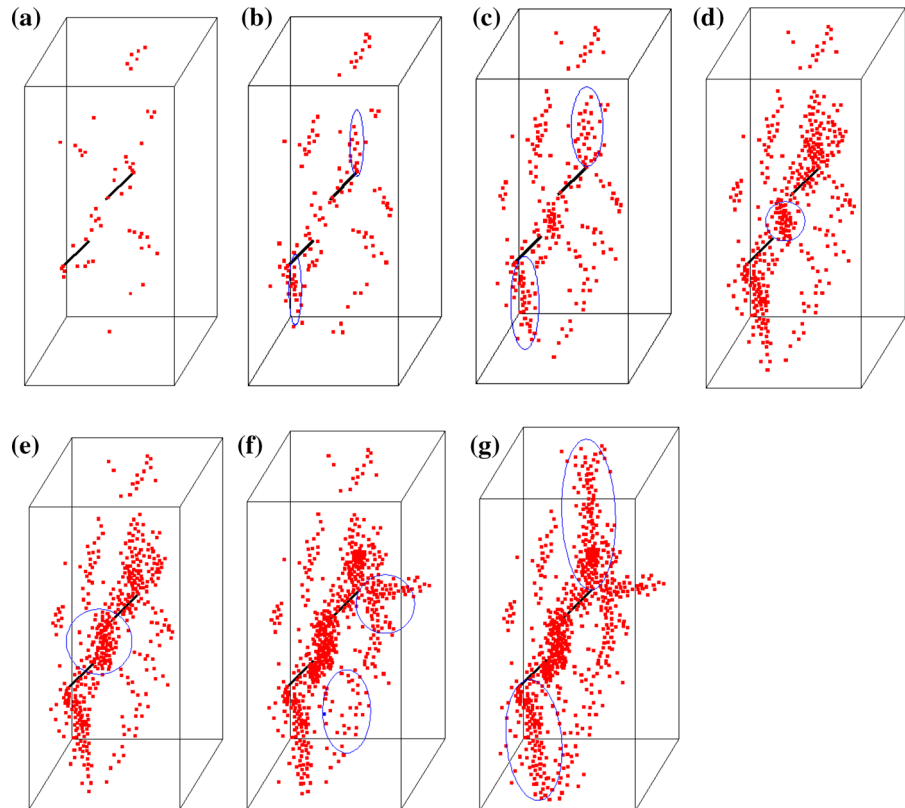
$\sigma_1 = 3.15 \text{ MPa}$ ($T = 381 \text{ s}$;
 Point B). **d** $\sigma_1 =$

3.178 MPa ($T = 385 \text{ s}$;
 Point C). **e** $\sigma_1 =$

3.357 MPa ($T = 406 \text{ s}$;
 Point D). **f** $\sigma_1 =$

3.465 MPa ($T = 419 \text{ s}$;
 Point E). **g** $\sigma_1 =$

3.518 MPa ($T = 425 \text{ s}$;
 Point F)



the variation characteristics of the apparent elastic modulus differ greatly from that of the uniaxial compressive strength, but they both depend heavily on the flaw geometries such as ligament angle and flaw angle.

- Eight different crack types were observed during the sample cracking progress, which were defined based upon their initiation mechanism and trajectories subject to the applied loading. They can be used to investigate the crack coalescence mode and failure mechanism during the sample cracking progress, which may contribute to study rock damage and fracture mechanism. According to the ultimate failure modes of flawed samples, it is found that various cracks among the eight crack types cover every sample's surface, of which size and location vary wildly.
- Seven modes of crack coalescence were analyzed during the cracking process, which can be classified as shear crack coalescence (S-mode), mixed shear/tensile crack coalescence (M-mode) and tensile crack coalescence (T-mode). Each crack coalescence has a specific AE behavior pattern. The

AE behavior pattern of S-mode coalescence consists of three stages, i.e. minor active stage, quiet stage and major active stage, while the AE behavior of the sample producing T1-mode coalescence is characteristic by three various peaks. It can be concluded that S-mode coalescence occurs when two flaws are almost colinear, which is in the condition of $\beta \leq \alpha \leq 75^\circ$. M-mode coalescence is produced when $60^\circ \leq \beta \leq 90^\circ$, and the tensile crack may become dominant with the increase of the ligament angle. However, the geometry of the overlapping ($\beta \geq 90^\circ$) makes the sample easier to produce T-mode coalescence.

- The crack coalescence and failure process of all samples were recorded in real time by using photographic monitoring and AE technique. Two results are obtained: firstly, the axial stress-axial strain gradually deviates from the original track and develops towards the axial strain, which is caused by continuously increasing damage subject to the increasing load; secondly, the bigger decline of the average modulus reveals the appearance of new cracks, which is accompanied with more active AE

behavior, such as the larger AE energy and more AE events.

Acknowledgments Financial support from the National Basic Research Program of China (973 Program) Granted No. 2014CB046904 and the National Natural Science Foundation of China Granted Nos. 41130742 and 51474205 are gratefully acknowledged.

References

- Bobet A, Einstein HH (1998a) Fracture coalescence in rock-type materials under uniaxial and biaxial compression. *Int J Rock Mech Min Sci* 35(7):863–888
- Brace WF, Bombolakis EG (1963) A note on brittle crack growth in compression. *J Geophys Res* 68:3709–3713
- Cai M, Kaiser PK, Martin CD (2001) Quantification of rock mass damage in underground excavations from microseismic event monitoring. *Int J Rock Mech Min Sci* 38:1135–1145
- Carpinteri A, Xu J, Lacidogna G, Manuello A (2012) Reliable onset time determination and source location of acoustic emissions in concrete structures. *Cem Concr Compos* 34:529–537
- Celestino SP, Piltner R, Monteiro PJM, Ostertag CPO (2001) Fracture mechanics of marble using a splitting tension test. *J Mater Civ Eng* 13:407–411
- Colombo S, Main IG, Forde MC (2003) Assessing damage of reinforced concrete beam using *b*-value analysis of acoustic emission signals. *ASCE J Mat Civ Eng* 5(6):280–286
- Dey TN, Wang CY (1981) Some mechanisms of microcrack growth and interaction in compressive rock failure. *Int J Rock Mech Min Sci Geomech Abstr* 18:199–209
- Fairhurst CE, Hudson JA (1999) Draft ISRM suggested method for the complete stress–strain curve for the intact rock in uniaxial compression. *Int J Rock Mech Min Sci* 36:279–289
- Feng XT, Ding WX, Zhang DX (2009) Multi-crack interaction in limestone subject to stress and flow of chemical solutions. *Int J Rock Mech Min Sci* 46(1):159–71
- Fowell RJ, Hudson JA, Xu C et al (1995) Suggested method for determining mode I fracture toughness using cracked chevron notched Brazilian disc (CCNBD) specimens. *Int J Rock Mech Min Sci* 32(1):57–64
- Germanovich LN, Dyskin AV (2000) Fracture mechanisms and instability of openings in compression. *Int J Rock Mech Min Sci* 37:263–284
- Haeri H, Shahriar K, Marji MF, Moarefvand P (2013) On the crack propagation analysis of rock like Brazilian disc specimens containing cracks under compressive line loading. *La Am J Solids Struct* 11(8):1400–1416
- Hoek E, Bieniawski ZT (1965) Brittle fracture propagation in rock under compression. *Int J Fract Mech* 1:137–155
- Jerome F, Sergei S, Georg D, Yves G (2009) Acoustic emissions monitoring during inelastic deformation of porous sandstone: comparison of three modes of deformation. *Rock Phys Nat Hazards* 2009:823–841
- Landis EN, Baillon L (2002) Experiments to relate acoustic emission energy to fracture energy of concrete. *J Eng Mech (ASCE)* 128:698–702
- Lei XL, Nishizawa O, Kusunose K, Satoh T (1992) Fractal structure of the hypocenter distribution and focal mechanism solutions of AE in two granites of different grain size. *J Phys Earth* 40:617–634
- Li YP, Chen LZ, Wang YH (2005) Experimental research on pre-cracked marble under compression. *Int J Solids Struct* 42:2505–2516
- Lockner D (1993) The role of acoustic emission in the study of rock fracture. *Int J Rock Mech Min Sci Geomech Abstr* 30:883–899
- Park CH, Bobet A (2010) Crack initiation, propagation and coalescence from frictional flaws in uniaxial compression. *Eng Fract Mech* 77:2727–2748
- Peng S, Johnson AM (1972) Crack growth and faulting in cylindrical specimens of Chelmsford granite. *Int J Rock Mech Min Sci Geomech Abstr* 9:37–86
- Petit JP, Barquins M (1988) Can natural faults propagate under mode II conditions. *Tectonics* 7:1243–1256
- Pettitt WS (1998) Acoustic emission source studies of microcracking in rock. PhD thesis, Keele University, Staffordshire, UK
- Sagar RV, Prasad RV, Prasad BKR (2013) Microcracking and fracture process in cement mortar and concrete: a comparative study using acoustic emission technique. *Exp Mech* 53:1161–1175
- Schiavi A, Niccolini G, Tarizzo P, Carpinteri A, Lacidogna G, Manuello A (2011) Acoustic emissions at high and low frequencies during compression tests of brittle materials. *Strain* 47(2):105–110
- Shen B, Stephansson O, Einstein HH, Ghahreman B (1995) Coalescence of fracture under shear stresses in experiments. *J Geophys Res* 100:725–729
- Tham LG, Liu H, Tang CA et al (2005) On tension failure of 2-D rock specimens and associated acoustic emission. *Rock Mech Rock Eng* 38(1):1–19
- Wong LNY, Einstein H (2006) Fracturing behavior of prismatic specimens containing single flaws. In: 41st US Rock Mechanics Symposium. Omnipress, Golden, CO, US
- Yang SQ, Dai YH, Han LJ (2009) Experimental study on mechanical behavior of brittle marble samples containing different flaws under uniaxial compression. *Eng Fract Mech* 76(12):1833–1845
- Yang SQ, Jing HW (2011) Strength failure and crack coalescence behavior of brittle sandstone samples containing a single fissure under uniaxial compression. *Int J Fract* 168:227–250
- Yang SQ, Ni HM, Wen S (2014) Spatial acoustic emission evolution of red sandstone during multi-stage triaxial deformation. *J Cent South Univ* 21(8):3316–3326
- Zhao LG, Tong J, Hardy MC (2010) Prediction of crack growth in a nickel-based superalloy under fatigue–oxidation conditions. *Eng Fract Mech* 77:925–938
- Zhou XP, Cheng H, Feng YF (2014) An experimental study of crack coalescence behavior in rock-like materials containing multiple flaws under uniaxial compression. *Rock Mech Rock Eng* 47(6):1961–1986